

Pearling Instabilities of Membrane Tubes with Anchored Polymers

Ilan Tsafrir¹, Dror Sagi¹, Tamar Arzi¹, Marie-Alice Guedea-Boudeville,²
Vidar Frette^{1,†}, Daniel Kandel¹, and Joel Stavans¹

¹ Department of Physics of Complex Systems,

The Weizmann Institute of Science, Rehovot 76 100, Israel

² Laboratoire de Physique de la Matière Condensée, URA 792, Collège de France
11 Place Marcelin Berthelot, F-75231 Paris CEDEX 05, France

We have studied the pearling instability induced on hollow tubular lipid vesicles by hydrophilic polymers with hydrophobic side groups along the backbone. The results show that the polymer concentration is coupled to local membrane curvature. The relaxation of a pearled tube is characterized by two different well-separated time scales, indicating two physical mechanisms. We present a model, which explains the observed phenomena and predicts polymer segregation according to local membrane curvature at late stages.

PACS numbers: 87.16.Dg, 68.10.-m

Single-component phospholipid membranes have been the focus of intense interest in recent years, as the simplest model system of biological membranes [1]. The latter are highly complex systems, comprised of a bilayer consisting of many types of lipids as well as a mesh of macromolecules such as proteins and polysaccharides, which participate in a large variety of cellular processes. A natural step to mimic this complexity in a simple model system is to study the association of polymeric molecules with self-assembled single-component phospholipid membranes [2].

Experiments with polymers, which associate with membranes by *anchoring*, have revealed changes in the bending moduli of bilayers of single-tailed surfactants [3], and striking morphological changes in vesicles [2,4,5]. Anchoring occurs by the penetration of a number of hydrophobic side-groups grafted along a hydrophilic backbone into a bilayer. Hollow tubular vesicles incubated in a solution of anchoring polymers having a polysaccharide backbone develop a pearling instability, above a threshold polymer concentration [6]. This instability was not observed with purely hydrophilic polymers, and was effected by hydrophobic groups alone (without the backbone), but only at concentrations five orders of magnitude higher than with anchoring polymers.

In this experimental and theoretical study we investigate the mechanisms responsible for the pearling instability. It has been suggested that the induction of curvature by the anchors, which sink into the membrane to a depth of half a bilayer, may constitute a mechanism which drives the pearling instability [2]. Our results show, however, that two independent mechanisms – spontaneous curvature and area difference – contribute to the pearling phenomena.

In our experiments, vesicles were made of stearoyl-oleoyl-phosphatidyl-choline (SOPC) with C_{18} alkyl chains. The polymer used was hydrophilic dextran with a molecular weight of 162,000 g/mol, functionalized both with palmitoyl alkyl chains and dodecanoic NBD chains

as fluorescent markers. The anchors, distributed statistically along the backbone (about 1 alkyl chain per 25 glucose units) are C_{16} long. On average there are about four persistence lengths between consecutive anchors. $1\mu\text{l}$ droplets of SOPC in a 7:1 chloroform-methanol solution (10 mg/ml) were placed on a glass coverslip forming small lipid patches. The sample was prehydrated for 20 minutes under water-saturated nitrogen, then hydrated with 0.1 mM potassium buffer at pH 6.5. A large number of hollow tubes with one or more lamellae formed after hydration, connected to the lipid patch. The latter constitutes a reservoir with which the tubes can exchange lipid molecules. Experiments were conducted at room temperature, insuring that the membranes were in a fluid-like state. This allowed free diffusion of both lipids and anchored polymers along the bilayers. A drop of polymer solution of a given concentration was introduced through one of the cell sides. The polymer was added after the tubes were formed, and we therefore assume that it anchored mostly on the outermost leaflet of the membrane. Its concentration on the membrane grew from zero as more and more chains anchored from solution. Events were observed by phase contrast and fluorescence microscopy and recorded on video. The fluorescent NBD markers attached to the anchors were excited with an argon laser (488 nm), and observed with a CCD camera.

We show in Fig. 1 snapshots of a tube undergoing pearling after addition of polymer. The instability typically starts near the end cap of the tube (Fig. 1a), and gradually propagates along the axis (Fig. 1b). Existing pearls become gradually more spherical (Fig. 1c). The rate at which pearls form depends on the number of lamellae in the walls of the tube, as well as on the concentration of polymer in the water (2–100 mg/l), varying from several seconds to many minutes. A salient feature of Fig. 1c is the increase in pearl size as the tube end is approached. This size gradient becomes much more pronounced at very long times, as Fig. 1d illustrates for another vesicle. The string of pearls actually separates

into a set of small, nearly-uniform spheres, and another group consisting of much larger spheres.

We have studied the onset of pearling by measuring the wavelength of the fastest growing mode, P , just above threshold, as a function of the radius of the unpearled tube, R_0 . Within experimental accuracy P is linear in R_0 , with a slope $k \equiv 2\pi R_0/P = 1.07 \pm 0.05$. This result agrees well both with the value $k = 1$ predicted by theoretical models based on induced curvature as the driving mechanism [7], and with experimental results on pearling instabilities in single-tailed surfactant systems [8]. In tension-induced pearling $k \approx 0.7$ [9], and thus our measurement excludes pearling due to polymer or flow-induced tension in our system.

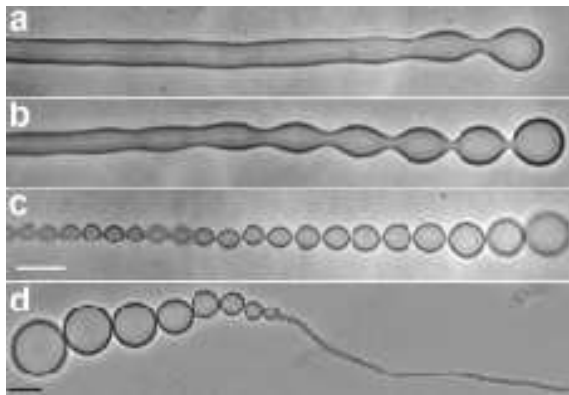


FIG. 1. Snapshots of a multilamellar tubular vesicle of SOPC undergoing a pearling instability: (a) 0, (b) 70 sec. and (c) 150 sec. after the onset of pearling. The concentration of polymer is below 2 mg/l . (d) Image of an inhomogeneous pearled structure at late stages of the instability, 900 sec. after the onset of pearling. The polymer concentration is below 100 mg/l , but much larger than in (a-c). The scalebar represents $20 \mu\text{m}$.

Polymers anchoring to one side of a membrane can in principle induce curvature by two mechanisms. The first is an increase in the area of the outermost monolayer into which anchors sink [10]. The second mechanism is a local deformation of the membrane which can be induced either by the anchors regarded as inclusions [11], or by the polymer backbone exerting an entropic pressure due to the constraint in its conformations [12]. These mechanisms form the basis of two models that describe the tendency of a membrane to display curvature: the area difference elasticity model (ADE) and the spontaneous curvature model (SC), respectively. Calculations of equilibrium shapes of vesicles with cylindrical symmetry based on both the SC and ADE models indeed yield pearled shapes of constant mean curvature called *Delaney surfaces* [13,14]. Thus, the equilibrium shape is not sensitive to the pearling mechanism.

Nevertheless, the dynamics of pearling may allow us to distinguish between the two mechanisms and reveal

their presence. This is reasonable, since the two mechanisms are characterized by well-separated relaxation time scales. Local induction of area difference or spontaneous curvature both decay diffusively [15]. The relaxation of spontaneous curvature is associated with polymer diffusion in the membrane. The relevant diffusion constant was measured for various macromolecules and is in the range of $1 \mu\text{m}^2/\text{sec} < D_{SC} < 5 \mu\text{m}^2/\text{sec}$ [16]. ADE relaxes via the sliding of one monolayer with respect to the other, and does not involve long distance diffusion of molecules. The diffusion constant associated with ADE can be estimated from dimensional analysis to be $D_{ADE} \approx K_0/b$, where K_0 is the compression modulus of the membrane, and b is the friction coefficient between the two leaflets of a bilayer. Experimental estimates of these parameters lead to $50 \mu\text{m}^2/\text{sec} < D_{ADE} < 500 \mu\text{m}^2/\text{sec}$ [15].

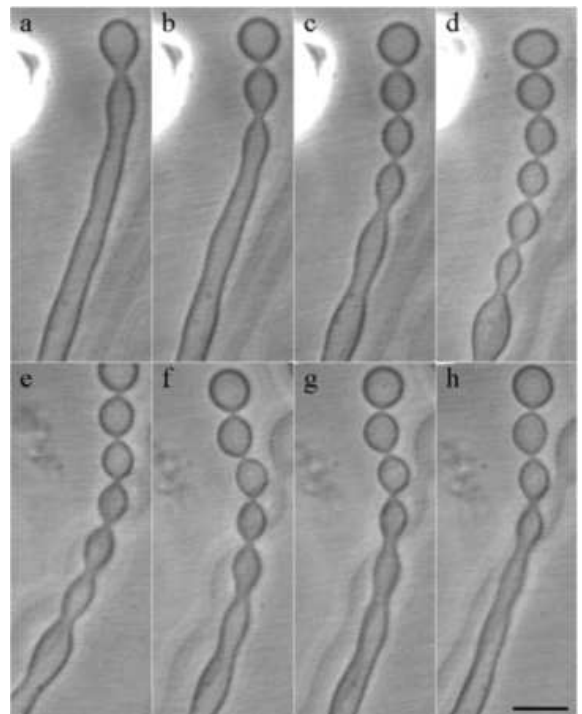


FIG. 2. Snapshots of a local pearling experiment. (a-d) show the formation of pearls as polymer is added from the micropipette at left. (e-h) show the subsequent opening of these pearls as polymer diffuses down the stem. Times are 2, 5, 8, 11, 42, 46, 54, and 65 seconds after the pipette is brought to the vicinity of the vesicle. Scalebar represents $10 \mu\text{m}$.

In order to study the relaxational dynamics, a micropipette was used to deliver locally a small volume (about $10^{-4} \mu\text{l}$) of polymer solution of concentration $20 - 100 \mu\text{g/ml}$ close to a particular tube (Fig. 2). Fluorescence images show that the polymer was indeed concentrated in a local region shortly after the injection. Pearling occurred, after an induction time in which en-

hanced undulations were observed (Figs. 2a-2d). The injection of the polymer was stopped after the pearled region increased to a length of order $100 \mu\text{m}$. The pearled region then shrank gradually (Figs. 2e-2h) as pearls opened up one at a time starting with those farthest from the region of polymer injection. This decay process took several minutes.

We measured the length of the pearled region (L) as a function of time during the decay process. For diffusive decay, we expect a linear dependence of L^2 on time, i.e., $L^2 \approx 2D(\bar{t} - t)$, where D is the relevant diffusion constant and \bar{t} is some constant. Figure 3 is a typical example of the dependence of L^2 on time. The system exhibits a diffusive behavior at early times with a diffusion constant of $D \approx 200 \mu\text{m}^2/\text{sec}$. At later times there is a sharp crossover to a much slower diffusive behavior with $D \approx 5 \mu\text{m}^2/\text{sec}$. Measurements on several tubes yield diffusion constants of the same order of magnitude. We view these results as evidence that both mechanisms are important in our system. At early times ADE dominates the unpearling kinetics, while at late times it is controlled by the slow diffusion of polymer molecules. To the best of our knowledge, this is the first kinetic measurement which differentiates between the ADE and local SC mechanisms.

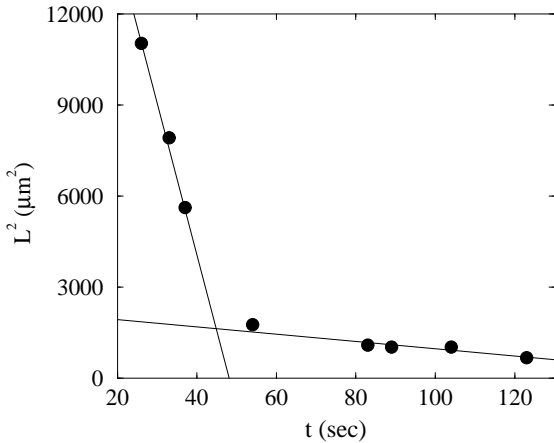


FIG. 3. Squared length, L^2 , of the pearled portion of a tube as a function of time, t , after the pipette is brought to the vicinity of the vesicle (circles). The straight lines are fits of the early and late evolutions to the equation $L^2 = 2D(\bar{t} - t)$. At early times $D \approx 200 \mu\text{m}^2/\text{sec}$, while at late times $D \approx 5 \mu\text{m}^2/\text{sec}$.

We now carry out a theoretical analysis of the pearling phenomena described above in the case of global application of the polymer (Fig. 1). We consider closed vesicles with polymer molecules partially covering the membrane only on the outer side of the vesicle, and assume that pearling is a result of the SC mechanism. All the predictions we outline below, except for the inhomogeneities in polymer concentration (see below), apply equally well

to the ADE model. In contrast with standard curvature elasticity models [14], the spontaneous curvature in our system is a *local* quantity, since it is induced by the polymer whose concentration may depend on position. We assume that the spontaneous curvature is proportional to the polymer concentration on the membrane; i.e., it is given by ρH_0 , where $\rho(\vec{r})$ is the fraction of the membrane area covered by polymer molecules at the position \vec{r} , and takes values in the interval $[0, 1]$. H_0 is the spontaneous curvature induced by full coverage of the polymer.

We further assume that the observed vesicle shapes are close to the equilibrium shapes under the constraints of constant vesicle volume and membrane area. These shapes can be obtained by minimizing the free energy of the membrane in the presence of the polymer. The simplest model for our system takes into account the curvature energy and the entropy of mixing of the polymer, leading to the following expression for the free energy:

$$F = \int dA \left\{ 2\kappa(H - \rho H_0)^2 + \frac{k_B T}{a^2} [\rho \ln \rho + (1 - \rho) \ln(1 - \rho)] \right\}, \quad (1)$$

where H is the local mean curvature, κ is the bending modulus of the membrane, a is the characteristic linear size of an anchored polymer molecule, and the integration is over the area of the membrane. We have measured the bending modulus κ using the pipette aspiration technique [17], and obtained $\kappa \simeq (20 \pm 5) k_B T$. Structures with radii smaller than optical resolution ($\sim 0.2 \mu\text{m}$) were observed in our experiments. This gives a lower bound of $H_0 \gtrsim 10 \mu\text{m}^{-1}$ on the spontaneous curvature induced by the polymer. Finally, a can be estimated as the radius of gyration of a polymer performing a two dimensional random walk on the membrane. Since the hydrophilic backbone is in water, we assume a good solvent in semi-dilute conditions, giving a radius between 40 and 80 nm.

We consider very long, cylindrically symmetric vesicles and ignore the existence of the end caps, since the length of most of the experimental tubes is larger than their radii by two orders of magnitude. To find the equilibrium configuration of the system, the free energy (1) was minimized with respect to the vesicle shape as well as the *local* polymer density, under the constraints of constant vesicle volume, membrane area and total number of polymer molecules, $\int \rho dA$.

Ideally, the equilibrium configuration of the system would have a homogeneous polymer distribution and a curvature $H = \rho H_0$ everywhere. Such a configuration minimizes the energy and maximizes the entropy simultaneously. This is indeed possible for a range of values of ρH_0 . For example, a vesicle with volume to area ratio of λ can have the shape of a cylinder of radius 2λ and curvature $H = 1/(4\lambda)$. Another shape, which corresponds to the same volume to area ratio, is a chain of identical spheres of radius 3λ with infinitesimally narrow necks

connecting them. In this case the curvature of the vesicle is $H = 1/(3\lambda)$ everywhere. In fact, the vesicle's curvature may take any intermediate value, $1/(4\lambda) < H < 1/(3\lambda)$, because for each of these curvatures there corresponds a Delaunay shape [18], with the same volume to area ratio. On the other hand, it is not possible to construct a shape of constant curvature for $H > 1/(3\lambda)$ or for $H < 1/(4\lambda)$.

In our experiment the polymer adsorbs onto the membrane gradually. Therefore, at the very early stages of the experiment $\rho < 1/(4\lambda H_0)$, and the shape of constant curvature which minimizes the energy is a cylinder of radius 2λ and curvature $H = 1/(4\lambda)$. This is consistent with our experimental observations. In principle, we also have to consider possible inhomogeneities in membrane curvature. However, our calculations show that for small ρ such inhomogeneities only increase the free energy.

At intermediate stages of the experiment the polymer concentration is in the range $1/(4\lambda H_0) \leq \rho \leq 1/(3\lambda H_0)$, and long vesicles are expected to have a Delaunay shape. Indeed, the shapes of vesicles we observe at intermediate stages of the experiment are similar to Delaunay shapes. Such pearl shapes have already been observed [6], and the importance of Delaunay shapes for this system has been discussed in the literature [13,19].

The situation becomes more interesting at late stages of the experiment when ρ exceeds the value $1/(3\lambda H_0)$. In this case, the best Delaunay shape is a chain of identical spheres of radius 3λ and curvature $H = 1/(3\lambda)$. However, a detailed calculation (to be presented elsewhere) shows that a configuration consisting of a chain of small spheres connected by infinitesimal necks to each other and to one large sphere has the lowest free-energy.

The small spheres have radius r_1 and polymer density ρ_1 , such that $r_1 = 1/(\rho_1 H_0)$. The energy of this subsystem vanishes, since its curvature is $H_1 = \rho_1 H_0$. The large sphere has radius r_2 and polymer density ρ_2 , and plays the role of a reservoir for the excess volume and polymer molecules. The ratios r_2/r_1 and ρ_2/ρ_1 can be calculated numerically as functions of the average polymer density, the area of the system and its volume. For the values of the model parameters discussed above we obtained $r_2/r_1 > 10$ and $\rho_2/\rho_1 < 0.3$. This ratio of the radii is consistent with the experimental configurations seen at long times, where chains of very small spheres coexist with few very large spheres, all connected by narrow necks (see Fig. 1d).

The strong inhomogeneity in polymer concentration predicted by the theory, is particularly interesting because it may show a qualitative difference between predictions of the local SC model and those of ADE models. The latter do not differentiate between polymer molecules and lipids; i.e., exchanging polymers with a larger number of lipids of the same total area does not change the energy. One can always use such exchanges to turn an inhomogeneous polymer distribution into a homogeneous one of higher entropy without changing the

energy of the vesicle. Hence, ADE models predict a homogeneous polymer distribution. In the local SC model, inhomogeneities in polymer distribution induce the same undesirable decrease in the entropy of mixing. However, inhomogeneities lower the energy, and our calculation shows that for reasonable parameter values, the reduction in energy does lead to sizable inhomogeneities. So far we have not been able to measure the polymer concentration on the membrane. We hope to do that in the future to test this interesting theoretical prediction.

We thank especially L. Jullien, for his help and encouragement. We also acknowledge useful exchanges with R. Lipowsky, E. Moses and S. Safran. This research was supported by The Israel Science Foundation administered by the Israel Academy of Sciences and Humanities - Recanati and IDB Group Foundation and The Minerva Foundation. V.F. gratefully acknowledges support from The Research Council of Norway (NFR).

[†] Present address: Dept. of Engineering, Stord/Haugesund College, Bjørnsonsgt 45, N-5528 Haugesund, Norway.

- [1] U. Seifert and R. Lipowsky, in *Structure and Dynamics of Membranes*, edited by R. Lipowsky and E. Sackman (Elsevier Science B.V., Amsterdam, 1995).
- [2] H. Ringsdorf, B. Schlarb, and J. Venzmer, *Angew. Chem. Int. Ed. Engl.* **27**, 113 (1988).
- [3] Y. Yang, R. Prudhomme, K. M. McGrath, P. Richetti, and C. M. Marques, *Phys. Rev. Lett.* **80**, 2729 (1998).
- [4] J. Simon, M. Kühner, H. Ringsdorf, and E. Sackmann, *Chem. Phys. Lip.* **76**, 241 (1995).
- [5] V. Frette, I. Tsafir, M. Guedea-Boudeville, L. Jullien, D. Kandel, and J. Stavans, *Phys. Rev. Lett.* **83**, 2465 (1999).
- [6] H. Ringsdorf, J. Venzmer, and F. M. Winnik, *Angew. Chem. Int. Ed. Engl.* **30**, 315 (1991).
- [7] P. Nelson, T. Powers, and U. Seifert, *Phys. Rev. Lett.* **74**, 3384 (1995).
- [8] S. Chaieb and S. Rica, *Phys. Rev. E* **58**, 7733 (1998).
- [9] R. Bar-Ziv and E. Moses, *Phys. Rev. Lett.* **73**, 1392 (1994).
- [10] B. L. S. Mui, H. G. Dobereiner, T. D. Madden, and P. R. Cullis, *Biophys. J.* **69**, 930 (1995).
- [11] S. Leibler, *J. Physique* **47**, 507 (1986).
- [12] R. Lipowsky, *Europhys. Lett.* **30**, 197 (1995).
- [13] H. J. Deuling and W. Helfrich, *Blood Cells* **3**, 713 (1977).
- [14] U. Seifert, K. Berndl, and R. Lipowsky, *Phys. Rev. A* **44**, 1182 (1991).
- [15] U. Seifert and S. A. Langer, *Europhys. Lett.* **23**, 71 (1993).
- [16] P. F. F. Almeida and W. L. C. Vaz, in *Structure and Dynamics of Membranes*, edited by R. Lipowsky and E. Sackman (Elsevier Science B.V., Amsterdam, 1995).
- [17] E. Evans and W. Rawicz, *Phys. Rev. Lett.* **79**, 2379 (1997).
- [18] J. Eells, *Math. Intelligencer* **9**, 53 (1987).
- [19] O. Y. Zhong-can and W. Helfrich, *Phys. Rev. A* **39**, 5280 (1989).